CALICE Analysis Note CAN-0XX
v1.0
April 12, 2018

Timing Measurement in the CALICE Analog Hadronic Calorimeter engineering prototype

The CALICE Collaboration [1]

Abstract

This note presents the results obtained with the CALICE *Analog Hadronic Calorimeter* engineering prototype at the SPS CERN testbeam campaign in 2015. The analysis presents the timing calibration and includes timing distributions for muon, electron and pion beams. The results are compared to several GEANT 4 version 10.1 physics lists.

[1] Corresponding author:
Eldwan Brianne; eldwan.brianne@desy.de

Contents

1 Introduction

Experiments at future lepton colliders require unprecedented jet energy resolution of 3-4% up to 250 GeV jet energies. The Particle Flow concept (PFAs) aims to achieve such

resolutions by combining measurements of the tracker and calorimeters. This requires exceptional granularity for the calorimeters. The CALICE Collaboration develops, builds and tests such calorimeters to fulfill the requirements imposed by PFAs.

One calorimeter concept is the Analog Hadronic Calorimeter (AHCAL) that consists of scintillator tiles of 3×3 cm^2 readout by Silicon Photomultipliers (SiPMs). Several prototypes with different absorbers, granularity and readout have been tested.

Apart from energy measurement, the aspect of precise timing measurement is being investigated. Timing measurements in a calorimeter can be used to reject out of time pile-up events. In addition, the high level of $\gamma\gamma \rightarrow$ hadrons background could be rejected by using timing information of the calorimeter in order to limit the impact of background events on physics measurements. Moreover, time information could be used to improve the energy reconstruction [1].

The CALICE Analog Hadronic Calorimeter (AHCAL) technological prototype [2, 3] has been installed in the SPS CERN facilities in July 2015 in order to provide measurements using plastic scintillators. The goal of this study is to improve our knowledge about hadronic showers especially about its time evolution and time correlations of layers within the calorimeter. This note presents the time calibration procedure of the AHCAL and the results obtained in muon, electron and pion beams in an energy range from 10 GeV to 90 GeV, as indicated in table 3.

2 Testbeam Setup

The testbeam setup at CERN in July 2015, at the SPS beamline H2, is shown in figure 1. The AHCAL is composed of 48 iron absorber plates in which 14 active layers are installed. The 10 first layers consist of single ECAL and HCAL Board Units (HBU) of a depth of around 10 X_0 ($\sim 1\ \lambda_\pi$) aiming to act as a shower start finder. The next four layers consist of 2 by 2 HBUs inserted in slots 11, 13, 21 and 31 of the absorber structure providing information about the development of pion showers at different depths. In total, the prototype has 3744 channels. It uses SiPM technology coupled to scintillator tiles of 3×3 cm^2 readout by an application specific integrated chip, the SPIROC2b [4]. The AHCAL detector is placed on a movable stage in order to be able to move the detector position relative to the beam for muon calibration runs.

Scintillator plates in front and back of the calorimeter are used as a trigger signal that is provided to the AHCAL DAQ to validate events [5]. Additionally, the coincidence signal from the scintillators is provided directly to several channels of the AHCAL in order to provide a reference time of the trigger as shown in table 4. A Cherenkov detector, at around 100 m upstream, was available to tag incoming particles.

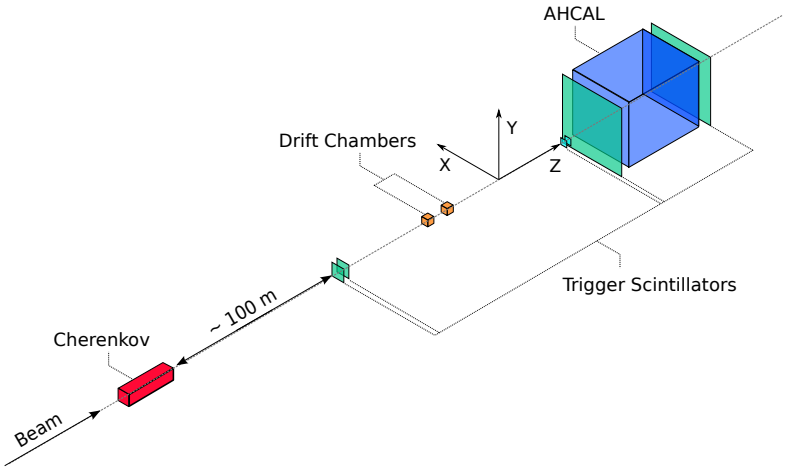

Figure 1 – Sketch view of the beamline setup at the CERN SPS H2 beamline in July 2015.

3 Simulation

The simulation model of the AHCAL prototype is based on the MOKKA [6] framework v08-05-01 and the new DD4HEP [7] framework v00-16, using the GEANT 4 v10.1 simulation. A right-handed coordinate system is used such that the Z-axis points in the beam direction and that the Y-axis is directed upwards. No beamline instrumentation is simulated except scintillator triggers in front of and behind the detector. A similar amount of material is achieved by filling the world volume with air and by adding 5.6 mm of lead ($\sim 1\ X_0$) directly at the calorimeter front face in order to account for missing upstream material. The beam gun is placed 1 m from the calorimeter front face and it is configured to generate single beam particles with a 2% momentum spread according to the beamline beam parameters [8]. All electron showers are simulated using the QGSP_BERT_HP physics list. Pion showers are simulated using QGSP_BERT, QGSP_BERT_HP and QBBC physics lists.

3.1 Geometry and Digitization

The AHCAL simulation model consists of 32 absorber layers and 14 active layers. Each absorber layer are made of stainless steel 17.2 mm thick. Each active layer is primarily composed of 1 mm steel cassette, 0.7 mm PCB, 2 or 3 mm scintillator strip or tile. The density and composition of the scintillator is taken as default provided in GEANT 4.

The digitization of simulated hits is very similar to the previous AHCAL physics prototype [9]. Individual calibration factors obtained from data are used to extract the light yield which is needed to model the statistical fluctuations of photons hitting a SiPM [10]. Saturation effects are also included using a global parameter, the number of pixels available on each SiPM type, as no measurement of the saturation curve is available. Most of the

tiles used are wrapped with a reflective foil such that crosstalk effects between channels can be neglected. For layers with no wrapping, a default value of 15% cross-talk is used. Noise is extracted from muon runs and overlaid onto simulated events. The timing of simulated hits is modeled as in the SPIROC2b, the energy from sub-hits in a cell is integrated over a sliding time window of 15 ns, if the energy sum of the sub-hits in this time window passes the energy threshold, the time of the sub-hit passing the energy threshold is used as the time of the simulated hit. To simulate detector resolution effects, the time of a simulated hit is smeared with a double Gaussian function, with parameters determined from data, and is convoluted with a Gaussian function with a sigma depending on the number of triggered channels in a chip parametrized from data (see section 5.7).

After the digitization, all simulated hits have the same format as raw data hits and are reconstructed with the same software chain that is used for data. To suppress noise hits, only hits above 0.5 MIP are considered in this study.

3.2 AHCAL Model Validation

Prior to the time analysis, the simulation and digitization were validated. Comparisons of electromagnetic interactions in the AHCAL are done as such interactions should be well described in simulation. Firstly, the comparison of the spectrum of a MIP-like particle traversing the AHCAL was done and is shown in figure 2a. The shape of the spectrum matches relatively well. The data appears slightly wider than for simulation because of channel-by-channel mis-calibrations that are not modeled in the simulation. The figure 2b shows the distribution of the extracted MIP calibration constant for single channels in data and simulation. Both data and simulation give a mean value around 1 MIP for the AHCAL indicating a good average calibration at the cell level. The higher values to the right that appear in the data have been checked and all channels present a good fit. The AHCAL simulation is slightly shifted to the right to higher values but is still reasonably close to unity.

Further comparison were made using the electron dataset. The figure 3 shows the hit energy spectra for 10 GeV electron showers in data and simulation. Hit energies up to 60 MIPs are well described by the simulation up to 10%. A small difference is noticeable around 20 MIPs because of overestimated intercalibration factors between high gain hits and low gain hits that shift the hit energy to slightly higher values. The simulation is underestimating the hit energy by a large factor over 60 MIPs. It is similar at higher beam energies. The underestimation in simulation of the hit energy comes from an incorrect value of the number of effective pixels used in the saturation function to saturate hits in the simulation. This number is too small thus saturating the simulation to lower hit energies.

The figure 3b shows the mean energy sum $< E_{sum} >$ as a function of the electron beam energy between 10 and 50 GeV in data and simulation with different cross-talk parameters.

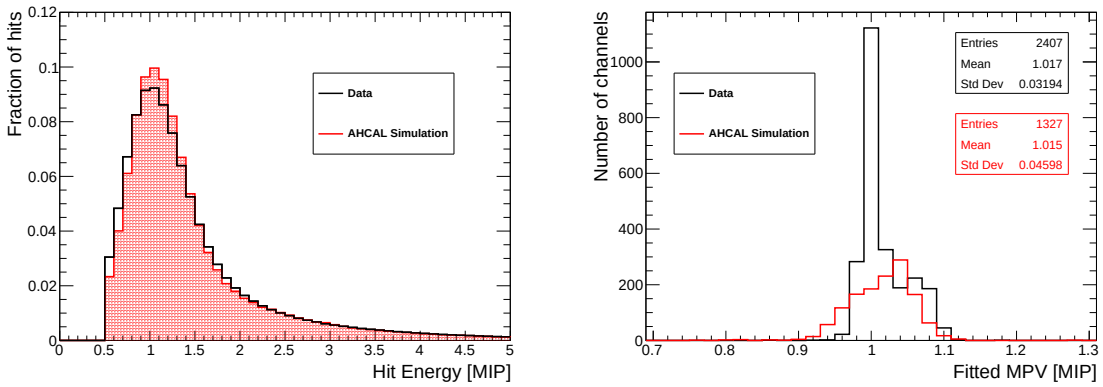

(a) **(b)**

Figure 2 – a) Hit Energy Spectra for the complete AHCAL for muon like-track hits for both data and simulation. b) Distribution of the fitted MIP value in single channels of the AHCAL for data and simulation.

The mean is obtained from the mean of the distribution. The visible energy for data agrees within the simulations for 10, 15 and 20 GeV electron energy and seems to agree better with the 10% cross-talk simulations. For higher energies, the data deviates significantly to lower values due to the presence of the long tail left of the distribution that may be related to contamination by lower energy electrons and that the simulations cannot describe. In addition, the curve does not look linear as one would expect, this is probably due to saturation effects that are not corrected and predominant to high electron beam energies.

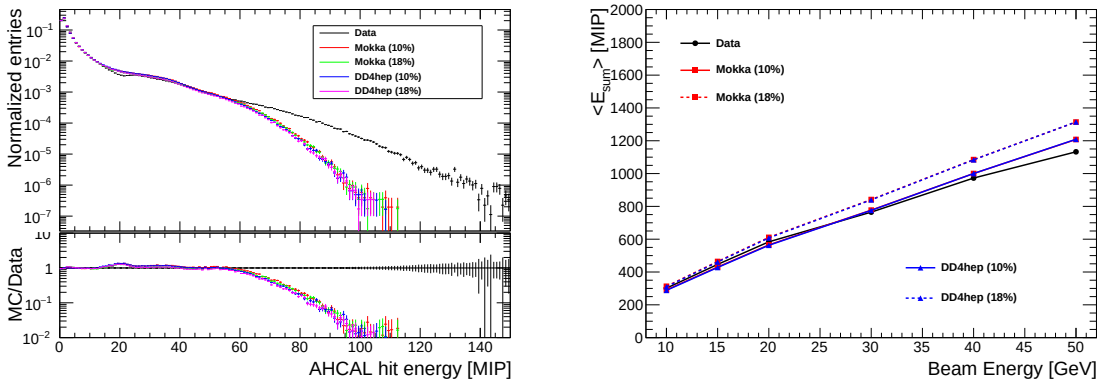

(a) **(b)**

Figure 3 – a) Electron hit energy spectra for data and simulation for 10 GeV beam energy. The different colors corresponds to the variation of the cross-talk parameter in the simulations between 10% and 18%. b) Comparison of the mean energy sum in the AHCAL as function of the beam energy for electron data and simulations with different cross-talk parameters. Simulated with QGSP_BERT_HP in GEANT 4 v10.1.

The simulation does not describe perfectly the data especially for higher electron beam energies but still reflect the data around 10-20%. However, the description of electromagnetic showers in simulations is deemed satisfactory for the study of the time development of hadron showers.

4 Event Selection

4.1 Muon selection

To select muons, an event pre-selection and a track finder [10] selection is performed. A cut on the number of hits in the AHCAL is done at 20 as the number of hits should be around 1 per layer for a MIP-like particle plus the number of noise hits expected in the detector. The track finder algorithm selects AHCAL towers of hits in the same $x : y$ position and it rejects AHCAL towers that contains less than a certain number of hits. In order to select muons or punch-through pions, a straight track of at least 7 hits is required in the whole AHCAL. This assumes that the calorimeter was perfectly perpendicular to the beam, therefore any tilted tracks would be missed. In addition, to reject late pion showers, no more than 2 hits are allowed per layer to account for some flexibility with noise hits. A summary of the muon selection is shown in table 5.

4.2 Electron selection

Electron events are needed to validate the timing behavior in simulation as well as the detector simulation model. It is important to have a clean sample of electrons to cross-check the timing calibration. An electron selection is done using the beam instrumentation and layer information. Events with a Cherenkov tag are used. The energy deposit in the first three AHCAL layers ($E_3 + E_4 + E_5$) must be over 10 MIPs. A box cut on the number of hits and the center of gravity in the z direction is done. As the number of hits in a electron shower is proportional to the shower energy, this cut is energy dependent. The energy deposited in the last two layers relative to the energy deposited in the calorimeter ($(E_{13} + E_{14})/\Sigma E$) is required to be under 1% to reject pion showers and to contain the electron shower. The electron selection is summed up in table 6.

4.3 Pion selection

The goal of the pion selection is to reject punch-through pions, muons and possible electron contamination as these events would be instantaneous. The events without a Cherenkov tag are selected. The number of hits required per event needs to be over 20 to reject most muons or punch-through pions without cutting on the center of gravity in z in order not to bias the start of the pion shower. The energy fraction deposited in the two last AHCAL

layers must be over 1% in order to ensure that pion showered and reject possible electron showers. The number of hits in the two first AHCAL layers $N_3 + N_4$ must be under 5 to mitigate possible particle contamination from electrons. In addition, multiple particle events were observed in the data. As no beam instrumentation could be used for rejecting these events, a rejection method based on the hit time information was developed. The method is the following: all the hits in an event are placed and ordered in time; Then for each hit after 50 ns, a timing window of 30 ns is looked after. The number of hits in that window is counted. If the number of hits is over 5, it is classified as a *late cluster*. The event is rejected if there is at least one late cluster. This method works because if an event has several particles, the time reference of the event is generated by the first particle. Therefore, the second particle will have all the hits late relative to the time reference and thus the event will be rejected. The multi-particle event rejection has been checked on simulated data and affects the selection between <0.1% up to 2% from 10 to 90 GeV pions. These multi-particle events are greatly suppressed in data. The number of events removed varies between 0.1% and 1% depending on the beam energy. Due to the calorimeter not being fully equipped thus providing limited information, some contamination may remain in the data. The table 7 shows the selection cuts for the pion data.

5 Timing calibration of the AHCAL

In a first time, the muon data is used to determine the parameters for the timing calibration. Muons are used because the process they induce is instantaneous. In a second step, the calibration is cross-checked using the electron data as also EM showers are instantaneous. This enables a verification of the time calibration procedure and may reveal effects that are not present in the muon data.

5.1 Time recording in the SPIROC2b

The time information provided by the SPIROC2b in the data is in TDC units. Similar to the ADC scale, it would be difficult to compare directly channels using the TDC unit. The TDC information needs to be interpreted into a common unit of time, the nanosecond. The TDC information of each channel can be converted into nanoseconds following the simple schematic shown in figure 4.

In order to determine the ramp slope, the starting point or pedestal of the ramp and the endpoint of the ramp are measured. Since the SPIROC2b has two TDC ramps, each defined by a BXID parity (even or odd), two slopes need to be extracted per chip. In addition, each channel can store up to 16 events called memory-cell. Each memory-cell is different thus 16 calibration values or pedestal are needed per channel. The extraction of the slope and the determination of the pedestal is described in the following sections.

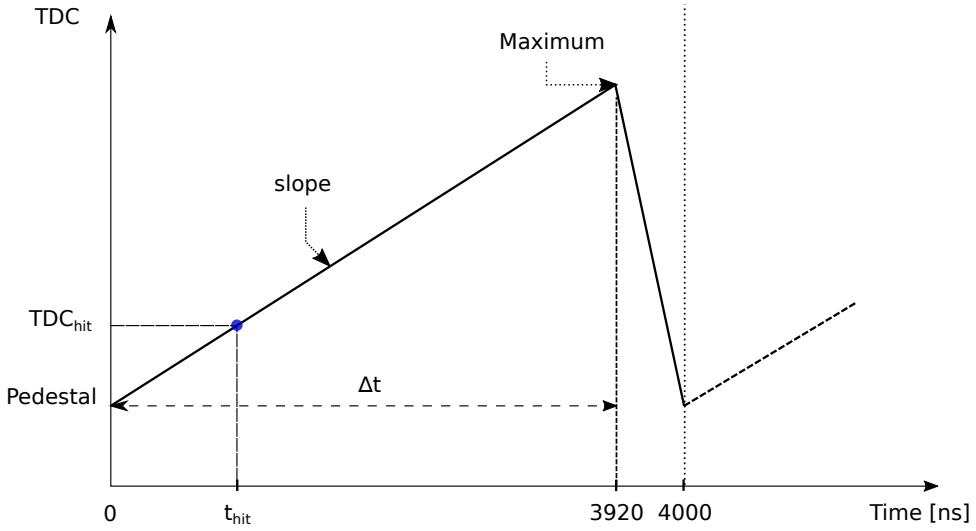

Figure 4 – Schematic of the TDC ramp in the SPIROC2b used in testbeam with a slow clock of 250 kHz. The slope of the ramp is Δ_t/(Max-Ped). The time of the hit is then calculated as the following: t_{Hit} = slope × (TDC_{Hit} - Ped).

5.2 Timing calibration procedure

The timing calibration procedure of the AHCAL is quite tedious and requires a lot of steps. An overview of the steps performed for the time calibration of each individual AHCAL channels is shown in figure 5.

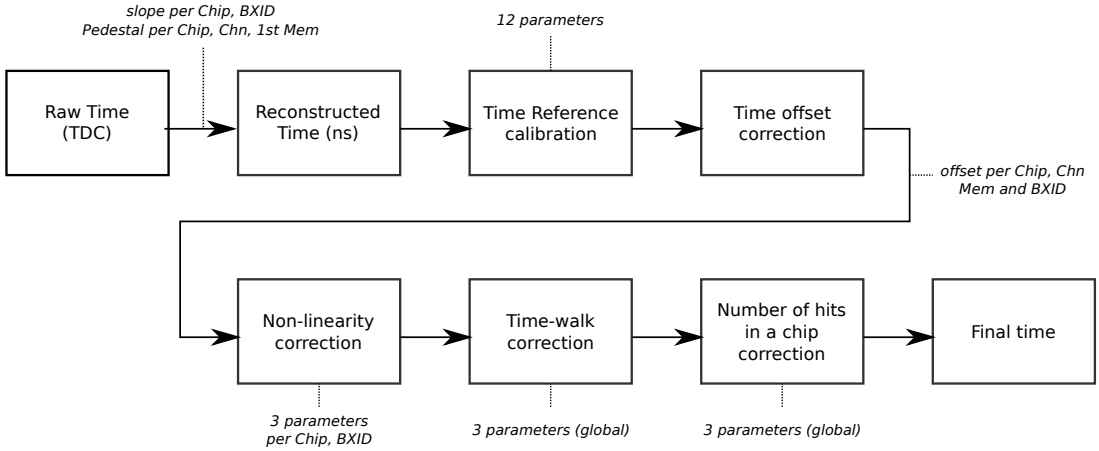

Figure 5 – Overall view of the different steps performed for the AHCAL timing calibration. In total, more than 20000 constants are needed.

5.3 Slope and Pedestal extraction

To reconstruct the time in a channel, the TDC value measured needs to be converted into nanoseconds. The slope is calculated as

$$s\,[\mathrm{ns/TDC}] = \frac{3920}{a-b} \tag{1}$$

where s is the TDC ramp slope, a is the endpoint of the TDC ramp and b is the start point of the TDC ramp that is referred in the following as the pedestal. The total length of the ramp is 3920 ns instead of the expected value of 4000 ns due to a deadtime of around 2% [11] induced by the multiplexer that switches between the two ramps.

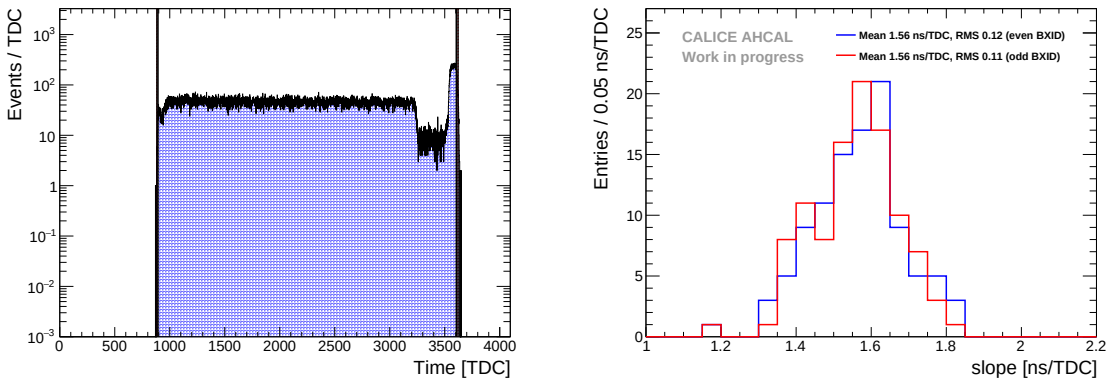

(a) **(b)**

Figure 6 – a) TDC spectrum of a typical chip. The black lines indicate the fitted Max and Pedestal parameters for this chip. The yellow bands represent the uncertainty on the extraction of the parameter a and b. The extracted parameters are $s = 1.47 \pm 0.01$ ns/TDC, $b = 888 \pm 5$ TDC and $a = 3613 \pm 8$ TDC. b) Distribution of the fitted slopes for even and odd bunch-crossing IDs. $\mu_{odd} = 1.564$ ns/TDC, $\mathrm{RMS}_{odd} = 0.121$, $\mu_{even} = 1.556$ ns/TDC, $\mathrm{RMS}_{even} = 0.113$. In total, 208 TDC slopes were extracted.

At a first order, the slope of the TDC ramp is assumed to be linear. The parameters a and b are extracted from the TDC spectrum of a channel per chip and BXID parity using only the first memory-cell as shown in figure 6a. The TDC ramp slope does not depend on the memory-cell as the memory-cell only introduce an offset on the parameters a and b. A total of 208 slopes have to be extracted for the testbeam setup.

The extracted values for the slopes are shown in figure 6b. They are in the expected range of 1.6 ns per TDC bin due to the limited dynamic range provided by the chip, around 2500 TDC bins for 4 μs.

5.4 Time delay correction

The time reference of the trigger is delayed compared to the muon passing through the detector because the length of cables and the trigger electronics logic. Therefore, the time offset of the time reference is determined from data. Muons are instantaneous particles thus the time of the first hit distribution for each channel, memory cell and BXID should peak at 0 ns.

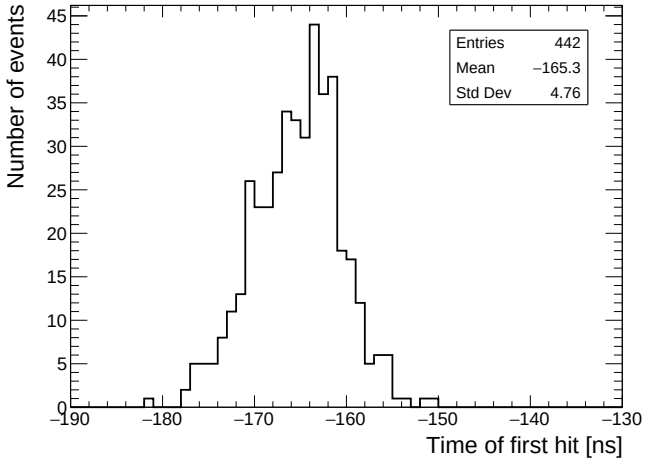

Figure 7 – Time of first hit distribution for a single channel (Chip 236, Chn 21, Mem 01, BXID 1). An offset of -165.2 ns is determined for this channel.

A shifting procedure of the time of the hit relative to the time reference for each channel, memory-cell and BXID parity is performed. This is done to take into account the delay time of the trigger due to cabling and the trigger electronics as well as possible differences in channel pedestals. Only memory-cells containing more than 100 events are considered. The histogram range of the time of the hit relative to the time reference is reduced iteratively until the RMS of the distribution is under 10 ns. This value was chosen because it corresponds to more than 3 sigma of the time reference uncertainty. The mean of the histogram is then used as the time offset value. An example of a single channel is shown in figure 7.

In total, 21040 individual offsets are extracted from data. The mean value of the time offset is around -150 ns which is around the expected value considering the cabling length and the trigger logic delay.

5.5 Non-linearity correction

The time calibration relies on the linearity of the TDC voltage ramp in the *SPIROC2B*. This assumption is not entirely reliable as described in [12, 11]. The voltage slope shows a slight kink around the middle thus leading to a non-linear ramp. For this, a correction of

the non-linearity is applied. Since the time reference is determined from a non-linear TDC ramp and it can't be corrected due to the lack of external time reference, the position of T_{hit} - T_{ref} on the ramp is corrected. The non-linearity correction results in an improvement in the timing resolution (RMS) of the AHCAL by about 5.1%.

5.6 Time-walk correction

The time-walk effect is due to the presence of an energy threshold that induces a time shift between a small amplitude signal and a high amplitude signal. Small amplitude signals will systematically trigger at a later time than high amplitude signals for a shaper that makes the signals peak at the same time. A time correction is determined by looking at the time of the first hit as a function of the amplitude of the hit. This may be particularly relevant for late energy depositions in hadron showers that comes generally from neutrons depositing little energy in the calorimeter. An improvement of around 3% is achieved on the time resolution of the AHCAL.

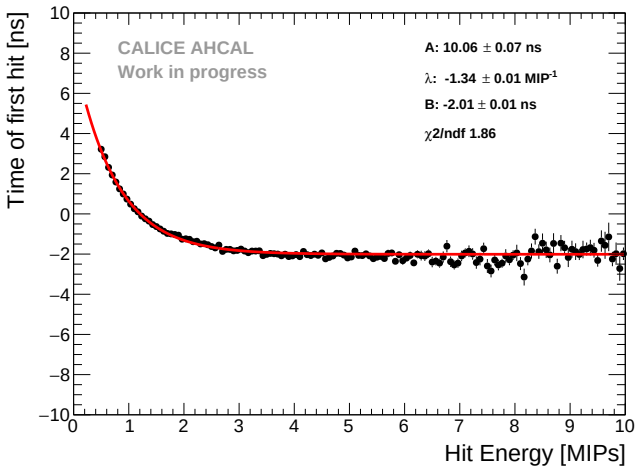

Figure 8 – Time of first hit as a function of the hit energy. A difference up to 6 ns is seen between small and large amplitudes. Time-walk correction extracted from data. The fit function is of the form $A \times e^{-\lambda x} + B$.

5.7 Number of triggered channel in a chip correction

The mean time of first hit as a function of the number of triggered channels over 0.5 MIP in a chip is shown in figure 9. A time shift up to 20-40 ns can be seen depending on the number of triggered channels in a chip. The cause of the observed effect is most likely due to an element in the chip called a *delay box* that gets unstable with a high charge going through the chip. This chip element is responsible for the hold signal of the TDC ramp

in the chip. The hold signal is delayed, and thus a higher TDC ramp value than the one expected is sampled.

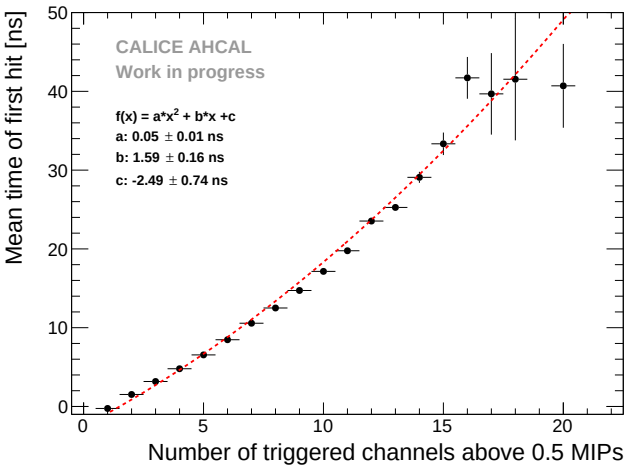

Figure 9 – Mean time of the first hit as a function of the number of triggered channels above 0.5 MIP in a chip. The mean time shift upwards with the increase of triggers leading to large tails in the time distribution. A second order polynomial fit is done for the time correction shown by the red dashed line.

In order to determine a reliable time correction, the time correction parameters are determined combining all the electron data. This effect may be chip-dependent and the parameters for the correction may differ from chip to chip. However, the limited amount of data does not allow to determine a correction function for each chip. Therefore, a global function is used to correct the time in the data.

6 Results

6.1 Systematic uncertainties

Systematic uncertainties need to be evaluated in order to perform a significant assessment of differences observed between data and simulations. Several possible sources were identified:

- Non-Linearity correction: A non-linearity correction is determined from data with a limited accuracy lead to a systematic uncertainty. The residuals of the correction give a systematic error at the level of 0.2 ns.
- Time walk correction: Similarly to the non-linearity correction, the systematic error obtained from the residuals of the time walk correction is in the order of 0.2 ns.

- Number of triggered channels correction: The correction for the number of triggered channels over 0.5 MIP in a chip results in a residual on the mean time of the first hit in the order of 1 ns. This systematic error is the most dominant over all other uncertainties. For the time of first hit distribution, a systematic uncertainty is applied bin-by-bin for electrons and pions in the region of -30 ns to 30 ns. Outside of this region, a systematic error of 50% is taken.

- AHCAL energy scale: The energy scale of the AHCAL was determined using the muon dataset. A systematic uncertainty on the MIP scale of around 3.6% was derived by dividing the muon sample in odd and even run numbers and by looking at the average spread of the fitted MIP value for both subsamples. This is converted to an uncertainty in time using the mean time of first hit as a function of the hit energy using the QGSP_BERT_HP physics list. At 0.5 MIP, this results in an uncertainty of 0.1 ns. For hits above 1 MIP, the uncertainty is below 0.05 ns.

- Global time smearing parameters: A global time smearing parametrization is used from muon data to smear the time in simulation. A bin-by-bin systematic error is applied to the time of first hit distribution to take into account the difference with a layer-wise time smearing parametrization.

- Number of triggered channels in a chip parametrization: A smearing parametrization of the width of the time distribution as a function of the number of triggered channels in a chip is obtained from electron data. An error band on the width was obtained by comparing all electron energies as explained. This is applied to simulation for systematics.

- Determination of the offset to $t = 0$: For simulation, the time shift per layer is calculated using a time of flight correction $T_{of} = \frac{z_{layer}}{c}$ with c the speed of light and z_{layer} the z position of a layer. For this, an uncertainty of 3 mm corresponding to the scintillator thickness is taken in z corresponding to 0.01 ns uncertainty in timing.

- Cross-talk: No measurement for optical cross-talk between tiles is available and from previous measurements, it varies between 10% and 18%. The cross-talk value induces a different number of hits in the detector thus has an impact on the width of the time of first hit distribution. The variation of this parameter in the simulation for the layers 4 to 10 is used for systematics.

- Absolute number of events: In the pion data, some possible contamination from multi-particle events may be present still after the selection. Thus, the number of true pion events is not known. A cluster time rejection method rejects up to 1% of events in the data. A conservative uncertainty of 10% on the data normalization is assigned when comparing data to simulation for the time of first hit distribution.

The systematic uncertainties are added in quadrature for the full systematic uncertainty assuming no correlation between uncertainties. For the mean time of the first hit as a function of the hit energy and as a function of the hit distance to the shower center of gravity, the systematic uncertainty is resulting at 0.3 ns for muons and 1.09 ns for electrons and pions. The table 1 sums up the systematic uncertainties used in the analysis.

Table 1 – Summary of systematic uncertainties.

Uncertainty source	Full uncertainty
Non-linearity correction	0.2 ns
Time-walk correction	0.2 ns
Number of triggered channels correction	1 ns / bin-wise (e/π)
Energy Scale	0.05-0.1 ns
Time of flight offset	0.01 ns (MC)
Cross-talk parameter	10-18% (MC)
Global time smearing parameters	bin-wise (MC)
Number of triggered channels in a chip parametrization	bin-wise (MC)
Multi-particle events	10% (π)
Systematics combined	
data-MC ToFH distribution	bin-wise (e) - bin-wise + 10% (π)
data-MC vs hit energy	0.3 ns (μ) - 1.09 ns (e/π)
data-MC vs hit distance to shower CoG	0.3 ns (μ) - 1.09 ns (e/π)

6.2 Timing of muon and electron beams

Firstly, the comparison of the time of first hit distribution for muons between data and simulations is shown in figure 10. The comparison shows that in the range of -20 ns to 20 ns, data and simulation agree well within the uncertainties. However, over 20 ns (and below -20 ns), the tails of the simulation don't agree with data. This is due to the noise implementation in simulation that is not perfectly reproduced. In addition, the time of distribution has been checked layer-by-layer and compared to simulations. Similarly, the agreement between data and simulations is best in the range of -20 ns to 20 ns and the tails are not perfectly reproduced in simulation.

Secondly, to further validate the time simulation, comparisons with electron data has been done. The figure 11a shows the comparison of the time of first hit distribution for 10 GeV electrons in data and simulation. The errors bars in the simulation are obtained by varying the cross-talk parameter between 10% and 18%, taking into account the global time smearing parametrization uncertainty and from the uncertainty of the parametrization of

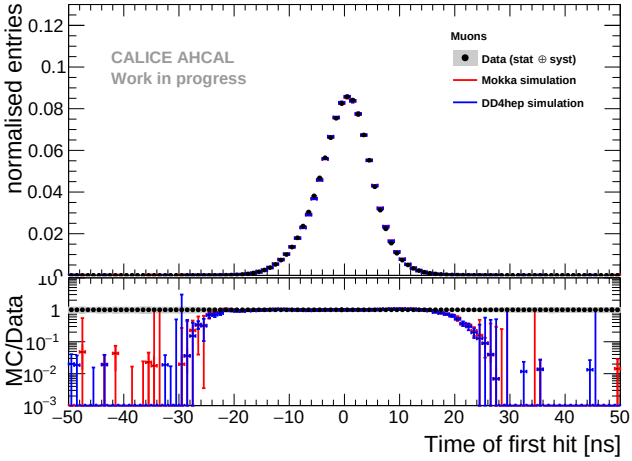

Figure 10 – Time of first hit distribution for muons in data and simulation between -50 and 50 ns. The grey area represents the statistical uncertainty of the data. The error bars of the simulation are obtained by varying the cross-talk parameter between 10% and 18% and taking into account the error of a global time smearing parametrization.

the increase of the width of the time distribution as a function of the number of triggered channels in a chip. The last uncertainty is dominant over the other uncertainties. The simulation is systematically narrower than data. This is caused by the simulation having fewer hits in a chip than data which can be seen in figure 11b. The simulation is generally 10% to 20% lower than data in the region of 6 to 10 hits per chip. Overall, the simulation describes well the data within statistical and systematic uncertainties in the central region of -30 ns to 30 ns for all energies. The large fluctuations in the simulation are due to the parametrization of the increase of the width. However, the description of the tails of the time of first hit distribution in the simulation are well underestimated. Like for muons, this is due to the description of the noise in the simulation that is not perfectly reproduced.

6.3 Timing of pion showers

The figure 12 shows the time distribution of first hits compared with three different physics lists for 10 GeV pions. For the core of the distribution under 50 ns, overall, all physics lists describe relatively well the data within the systematics. From 10 to 50 GeV, the QGSP_BERT_HP physics list reproduces well the distribution. Above 50 GeV, the tail after 100 ns is also well described in the simulation, however, between 50 and 100 ns, the simulation slightly under-estimates the data although within the systematic uncertainty. The QBBC physics list tends to over-estimate the late tail by around a factor 2. This does not agree with the observations made in the T3B experiment [13] where the QBBC physics list agrees well with the time distribution for 60 GeV pions. It may be related to the use

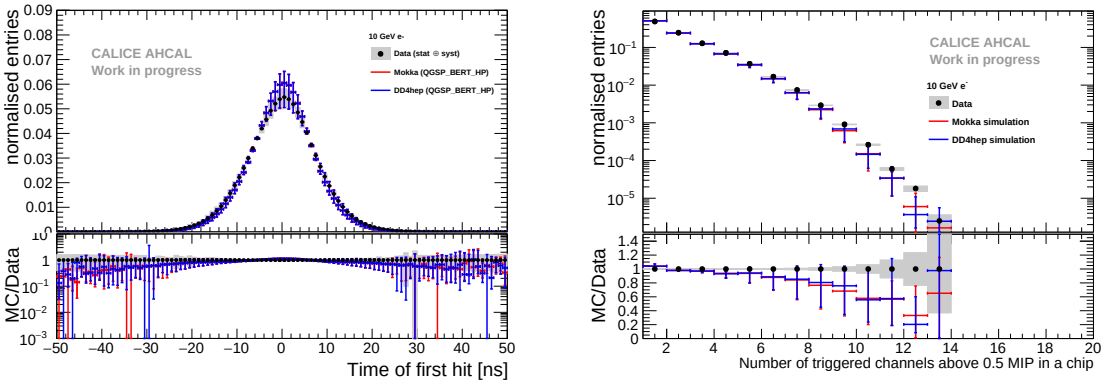

(a) **(b)**

Figure 11 – a) Comparison of the time of first hit between data and simulations for 10 GeV electrons. The grey area represents the statistical and systematical error of the data. Error bars in simulation are obtained by varying the cross-talk parameter between 10% and 18% and with the uncertainty on parametrization of the width of the time distribution as a function of the number of triggered channels in a chip. b) Comparison of the number of triggered channels per chip between data and MC for 10 GeV electrons. The grey area represents the statistical error of the data. Error bars in simulation are obtained by varying the cross-talk parameter between 10% and 18%.

of different GEANT 4 versions because the T3B experiment used GEANT 4 v9.4p03. For all pion energies, the QGSP_BERT physics list over-estimates the tail of the distribution by around a factor 10.

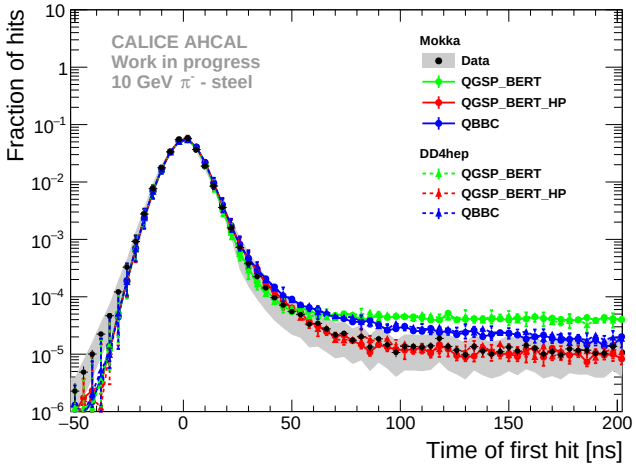

Figure 12 – Comparison of the time of first hit distribution for 10 GeV pions in data and three different physics list for MOKKA and DD4HEP simulations. The grey and color bands shows the statistical and systematic uncertainties.

The dependence in energy of the time of first hit has been studied in the following.

It is expected that there is no energy dependence for muon and electron beams as these are quasi-instantaneous. On the other hand, for pions, it is expected that low energy hits mostly coming from neutron signals in the calorimeter are delayed. The figure 13 shows the comparison of the mean time of first hit as a function of the hit energy in data and simulations for 10 GeV pions. For 10 GeV pions, the simulation reproduces well the data within the systematics. For higher pion energies, a difference is visible in the region 0.5 to 1.5 MIP where the simulation is above the data. Above around 3 MIPs, the data and simulations agree well. Firstly, a difference is visible between the QGSP_BERT and QGSP_BERT_HP physics lists mainly between hit energies of 1-3 MIPs but, in general, the difference is smaller than the systematic uncertainty on the data. Secondly, the QGSP_BERT and QBBC physics lists are very similar over the full hit energy range. Finally, all models show an increase of the mean time of first hit at small hit energies with higher beam energy. The data does not reflect this. This comparison study seems to confirm that low energy hits are responsible for delayed energy depositions in the calorimeter, most likely due to low energy neutrons from capture and spallation processes. Higher energy deposits occur mostly in the prompt part of the hadron shower.

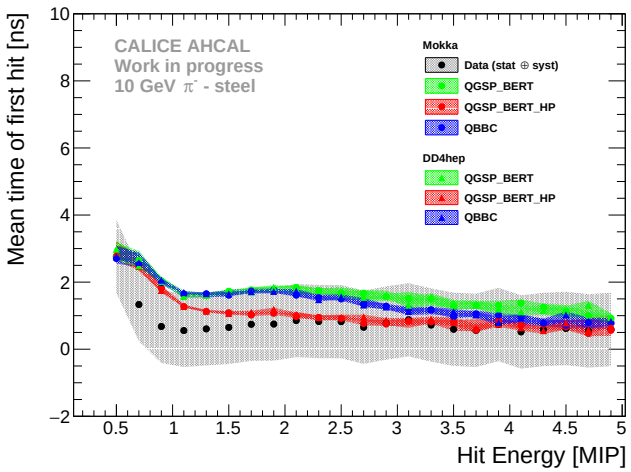

Figure 13 – Comparison of the mean time of first hit as function of the hit energy in data and simulations for 10 GeV and 90 GeV pions. The grey and color bands shows the statistical and systematic uncertainties.

The prompt component of a hadron shower is dominated by EM sub-showers and relativistic particles, whereas the delayed component is coming from mostly evaporation and spallation low energy neutrons. It is expected that the former is concentrated near the shower axis, while the latter, is spread out laterally as these neutrons can travel far away in the calorimeter before interacting. The radial dependence of the time of first hit of 50 GeV pion showers is compared to simulations as shown in figure 14. For the layers 3 to 10,

the QBBC and QGSP_BERT_HP physics lists reproduce well the data within systematics. The QGSP_BERT physics list agrees well under a 10 cm distance and then starts to deviate from data up to 4-6 ns at 23 cm. Concerning the layers 11 to 14, over the full energy range, the QGSP_BERT_HP physics list agrees the best with the data. The QBBC and QGSP_BERT physics lists agree with data up to around a 10 cm distance and then both lie above the data for higher distances, varing between few ns to 3-4 ns between 17 cm to 35 cm distance. This study shows that without the precision neutron tracking in simulation, too many late energy depositions are created that are spread far away from the shower axis.

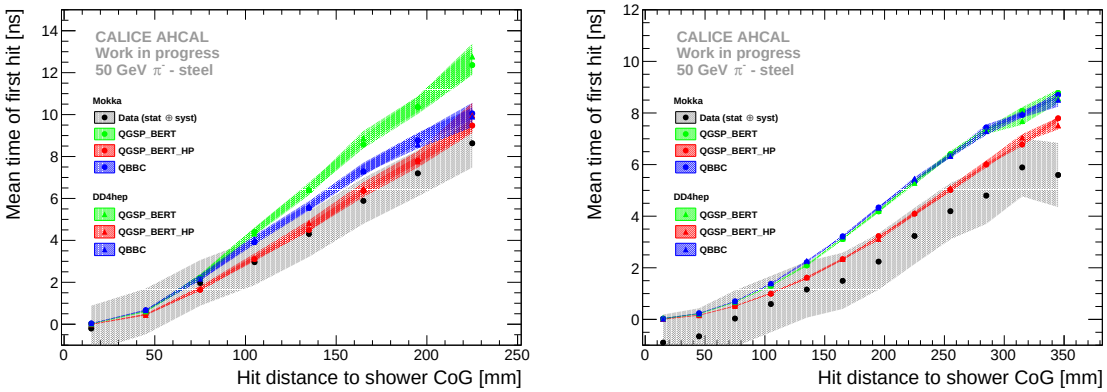

(a) Layers 3 to 10 **(b)** Layers 11 to 14

Figure 14 – Comparison of the time of first hit as function of the hit distance to the shower axis in data and simulations for 50 GeV pion for the layers 3 to 10 on the left and for layers 11 to 14 on the right. The grey and color bands shows the systematics.

The advantage of this studied prototype over T3B is the possibility to investigate time correlations between layers. For this study, the data below 50 ns is ignored as only the tail of the timing distributions is interesting.

The procedure is done by looking at each hit in layer i and checking in layer $i+1$ for a hit within a distance of 60 mm in the $x:y$ plane. If a hit is found, both times are plotted against each other. If more than one hit is found in layer $i+1$ within a distance of 60 mm, the closest in the $x:y$ plane is taken.

Two types of correlations were investigated, short and long. For the short correlation, the layers 6 and 7 were chosen, corresponding to 1 X_0 or 0.1 λ_π. As for the long, the layers 13 and 14 were selected, corresponding to 10 X_0 or 1 λ_π. These were chosen due to the fact that few layers were working properly. It is expected that EM sub-showers can lead to a correlation of hit times for the layers 6 and 7, while the layers 13 and 14 are far apart, and therefore would show less correlation of hit times. The hit times correlation is shown in figure 15 for the 50 GeV dataset.

The figures show that a correlation is visible in the data for both cases. To quantify

this, the following ratio is calculated

$$R = \frac{\int_{50ns}^{2\mu s} \int_{50ns}^{2\mu s} \frac{dN_i(t)}{dt_i} \frac{dN_j(t)}{dt_j} dt_i dt_j}{N_{tot}} \tag{2}$$

where N_{tot} is the total number of entries in the histogram and the nominator is the number of entries between 50 ns and 2 µs in the red box of the above figures.

The results show that 18.19% of the entries are in the red box region for the short correlation. This may come from EM sub-showers in the hadron shower. For the long correlation, 3.24% of the entries are in the red box region. This represents a substantial amount of hits that are correlated.

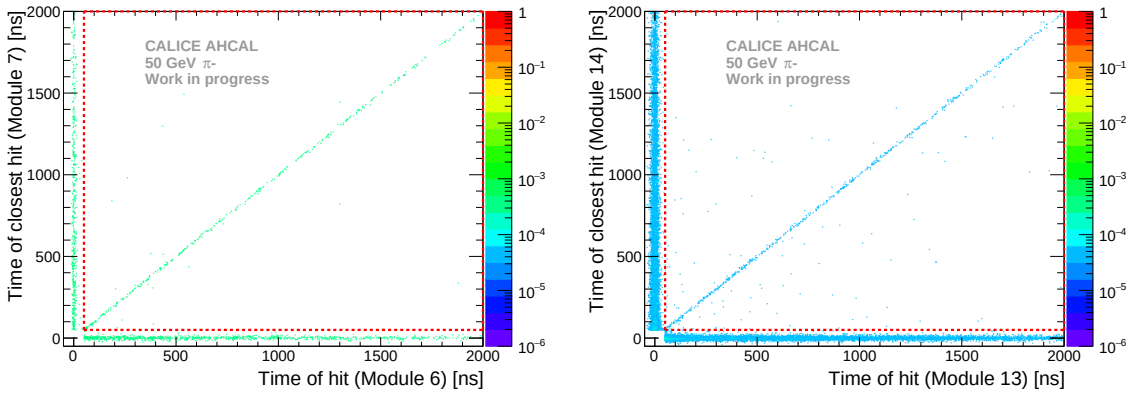

(a) **(b)**

Figure 15 – The left plot shows the time correlation between layer 6 and 7 separated by 1 X_0. The right plot shows the time correlation for layers 13 and 14 separated by 1 λ_π. Each bin is normalized to the number of entries in the 2D histogram. The red box represent the region of interest. Both plots show a visible time correlation.

This was compared to simulation using the QGSP_BERT_HP physics lists as shown in figures 16. In the same way, the number of correlated time hits was calculated and it is summarized in table 2. In general, the simulation possesses less correlated hits than in data for both type of correlations. In addition, the choice of the physics list is irrelevant for this observable as all physics lists give the same result within 0.1% maximum. Furthermore, the DD4HEP simulation has slightly less correlated hits, around 1%, at a short range than in the MOKKA simulation which is not understood but it is still within statistical uncertainties.

Comparing data and simulations, there is a large discrepancy for the short range correlation with a difference of around 15%. For the long correlation, the numbers also differ by around 3% but it is still within uncertainties. The reason for the discrepancy between data and simulation is not clear though it may come from the selection of the data that may be not good enough to reject multi-particle events, therefore providing more correlated hits

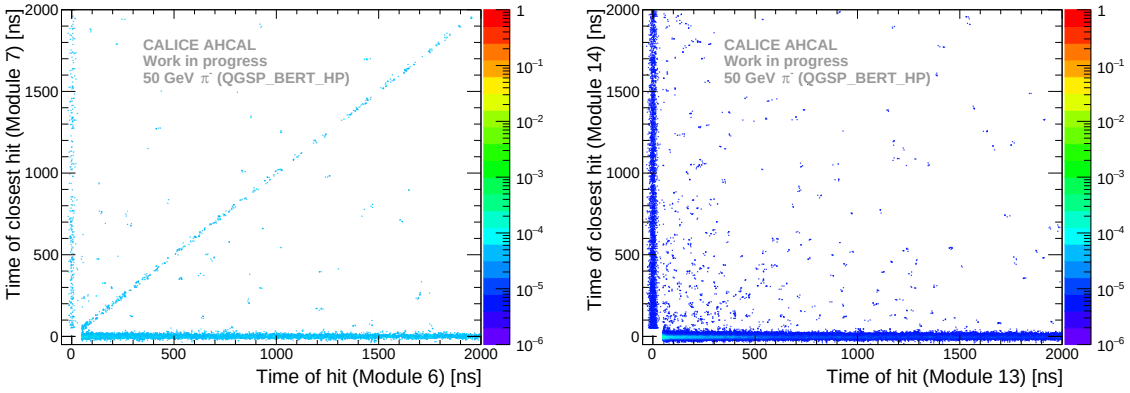

(a) Short correlation (QGSP_BERT_HP). **(b)** Long correlation (QGSP_BERT_HP).

Figure 16 – Hit timing correlations between layers 6 and 7 and layers 13 and 14 in the MOKKA simulation with QGSP_BERT_HP for 50 GeV pions. Each bin is normalized to the total number of entries in the 2D histogram.

than observed in simulation. More data, especially with a better detector to be sure to reject multi-particle events, is required in order to understand the origin of such correlations.

Table 2 – Table with fraction of events in the red box region as calculated with equation 2. The top is for MOKKA simulations, the bottom is for DD4HEP simulations. The quoted errors are only statistical errors.

Type	Short correlation [%]	Long correlation [%]
Data	18.19 ± 5.13	3.24 ± 3.79
QGSP_BERT	4.08 ± 3.44	0.65 ± 2.65
	3.01 ± 4.72	0.68 ± 3.25
QGSP_BERT_HP	4.1 ± 3.44	0.67 ± 2.65
	3.06 ± 4.72	0.71 ± 3.25
QBBC	4.09 ± 3.44	0.66 ± 2.65
	3.02 ± 4.72	0.69 ± 3.25

7 Conclusion

Time calibration of the AHCAL: The time calibration procedure of the AHCAL was presented. More than 20000 constants have been determined from data. A time resolution of 5.65 ns is achieved after a simple time calibration of the AHCAL. However, several effects from the front-end electronics can be corrected. The non-linearity correction ,related to the

non-linearity of the TDC ramp in the ASIC, improves the time resolution by around 5% and the time-walk correction, related to the slow shaper in the ASIC that delays low amplitude signals, improves the time resolution further by 3%. At the end, a time resolution of the order of 5 ns is achieved for minimum ionizing particles.

Validation of the time calibration: The timing calibration was cross-checked with the electron dataset recorded at CERN and the timing simulation has been validated. It was expected that a time resolution in the same order of magnitude or better than the time resolution obtained for MIPs would be achieved. However, due to the readout electronics that affects the time resolution as a function of the number of triggered channels in a chip, the time resolution for electron is worse with a value between 7.5 to 8.2 ns for beam energies between 10 and 50 GeV. This effect has been parametrized from data and implemented in the time smearing for the simulation. The simulation reproduces the data within 10-20% for all electron beam energies. However, the tails of the time distribution are not well reproduced due an imperfect implementation of noise hits. Nevertheless, this is considered good enough for looking at the time development of pion showers.

Timing of hadron showers: The timing of hadronic showers was studied. Firstly, the absolute time of first hit distribution has been investigated. The data shows a clear tail to late hits compared to MIP and electron time distributions. A comparison with simulation has been done for pion beam energies between 10 GeV and 90 GeV. The comparison showed that the QGSP_BERT_HP and QBBC physics lists agree well with the data. However, the QGSP_BERT physics list overestimate the amount of hits in the late tail by around a factor 10. Secondly, the energy dependence of the hit time has been studied. The data shows that late hits are concentrated at low hit energies below 1 MIP in iron. The comparison with simulation showed that for 10 GeV pions, the simulation agrees well with the data within the systematics uncertainty. However, for higher pion beam energies, a difference is visible at low hit energies between 0.5 MIP and 1.5 MIP where the simulation lies above the data. The difference seen may be due to the time correction of the data as a function of the number of triggered channels that is not perfect. For hit energies above 3 MIP, the data and simulation are in agreement. Thirdly, the radial dependence of the hit time has been investigated. This dependence has been looked at separately for layers 3 to 10 (single HBU) and layers 11 to 14 (2 by 2 HBU) due to a decrease of the mean hit time at the transition radius between the two type of layers. This has been studied in more details and concluded that this feature may be due to a dependence as a function of the start of the shower that showed that the radial dependence of the mean time of first hit decreases with deeper layers. The simulation reflects this feature as well. Anyhow, the data shows that late hits are mostly at a great distance from the shower axis, while prompt hits from electromagnetic

sub-showers and relativistic hadrons are predominant near the shower axis. A comparison between data and simulation has been carried out and showed that the QGSP_BERT_HP physics list agrees well with the data but the QBBC and QGSP_BERT physics lists agree with the data up to a hit distance to the shower axis of 100-150 mm and for higher hit distances to the shower axis, these physics lists tend to overestimate the late depositions by 1-3 ns. Fourthly, the longitudinal dependence of the hit time has been studied. This study concluded that there are no visible dependence for all beam energies. This is due to the timing resolution of the AHCAL that is too high. The simulation without time smearing shows that an increase of the mean time of around 1-1.5 ns is visible as a function of the layer depth. Finally, timing correlations between layers have been investigated. Short range (1 X_0 separation) and long range (10 X_0 or 1 λ separation) have been looked at. Time correlations are visible at short range as well as long range in different proportions in the data. In addition, a comparison of detailed simulations with data has been performed. It shows that in general, time correlations are reproduced in simulation but the amount of hits in data and simulation differ quite significantly. This may be due to the selection of the data that does not reject efficiently multi-particle events. More data and investigations to understand the origin such time correlations are needed.

Furthermore, the time resolution achieved in testbeam does not reflect the time resolution that could be accessible in an ILC running mode due to a different frequency of the slow clock (250 kHz in testbeam compared to 5 MHz at the ILC). By extrapolation, assuming that the time resolution scales linearly with the frequency of the slow clock, a time resolution of the order of 1 ns could be obtained in an ILC running scenario. The use of timing information could be a powerful tool to have to help in separating nearby showers in case of very busy events, for example in a ttH event. Timing information could also be used in a software compensation way by using timing bins differentiating electromagnetic sub-showers or relativistic hadrons and the hadronic late component, and weight each individual hit energy to improve the calorimeter energy resolution.

7 References

[1] A. Benaglia, E. Auffray, P. Lecoq, H. Wenzel, and A. Para, "Space-Time Development of Electromagnetic and Hadronic Showers and Perspectives for Novel Calorimetric Techniques," vol. 63, pp. 574–579, 04 2016.

[2] F. Sefkow and K. Krueger, "Towards a new AHCAL prototype," CALICE Collaboration Meeting, Arlington (Texas, USA), 14 Sep 2016 - 16 Sep 2016, Sep 2016.

[3] K. Krueger, "Prototype Tests for a Highly Granular Scintillator-Based Hadron Calorimeter," 16th International Conference on Calorimetry in High Energy Physics, Giessen (Germany), 6 Apr 2014 - 11 Apr 2014, Apr 2014.

[4] S. Callier, F. Dulucq, R. Fabbri, C. de La Taille, B. Lutz, G. Martin-Chassard, L. Raux, and W. Shen, "Silicon photomultiplier integrated readout chip (spiroc) for the ilc: Measurements and possible further development," in *2009 IEEE Nuclear Science Symposium Conference Record (NSS/MIC)*, pp. 42–46, Oct 2009.

[5] Kvasnicka, Jiri, "A Scalable Data Acquisition System for the CALICE Tile Hadron Calorimeter," *Conference Record IEEE*, 2016.

[6] P. Mora de Freitas and H. Videau, "Detector simulation with MOKKA / GEANT4: Present and future," in *Linear colliders. Proceedings, International Workshop on physics and experiments with future electron-positron linear colliders, LCWS 2002, Seogwipo, Jeju Island, Korea, August 26-30, 2002*, pp. 623–627, 2002.

[7] M. Frank, F. Gaede, C. Grefe, and P. Mato, "DD4hep: A Detector Description Toolkit for High Energy Physics Experiments," *J. Phys. Conf. Ser.*, vol. 513, p. 022010, 2014.

[8] "CERN North Area H2 beamline."

[9] The CALICE collaboration, "Construction and commissioning of the CALICE analog hadron calorimeter prototype," *Journal of Instrumentation*, vol. 5, no. 05, p. P05004, 2010.

[10] O. Hartbrich, *Scintillator Calorimeters for a Future Linear Collider Experiment*. PhD thesis, Hasylab, DESY, Hamburg, 2016.

[11] E. Brianne, "Studies of the front-end electronics of the Analog HCAL." DESY summer student report, 2012.

[12] O. Hartbrich, "Investigation of the time measurement capabilities of the SPIROC2b ASIC." DESY summer student report, 2011.

[13] F. Simon, C. Soldner, and L. Weuste, "T3B - an experiment to measure the time structure of hadronic showers," *Journal of Instrumentation*, vol. 8, no. 12, p. P12001, 2013.

Appendix

Table 3 – List of runs taken at SPS in July 2015.

Particle	**Energy**	**Runs**	**# Events**
μ^-	50 GeV	24016-24204	120,887,651
	150 GeV	24623-24662	15,534,328
e^-	10 GeV	24531-24576	38,028,438
	15 GeV	24507-24527	7,701,325
	20 GeV	24479-24504	10,498,554
	30 GeV	24454-24475	3,382,943
	40 GeV	24420-24448	2,665,843
	50 GeV	24404-24419	5,933,995
π^-	10 GeV	24266-24272, 24300-24317, 24381-24397	24,311,420
	20 GeV	24398-24400	N/A
	30 GeV	24259-24299, 24319-24380	10,120,753
	50 GeV	24212-24254, 24325-24357, 24580-24612	10,704,661
	70 GeV	24219-24242, 24365-24374	8,885,407
	90 GeV	24233-24287, 24331-24364	7,955,604

Table 4 – List of AHCAL channels used as time reference for this analysis. In this analysis, the time reference signals T_{12}, T_{13} and T_{14} are used.

Layer #	Chip Number	Channel	Comments	Name
11	169	29	noisy	T_{11}
11	177	23	broken	-
12	185	29	-	T_{12}
13	201	29	-	T_{13}
13	211	6	broken	-
14	217	23	-	T_{14}

Table 5 – Selection cuts for the muon runs.

Name	**Beam Energy**	**Cut**
Preselection	All	0 mm $< cog_z <$ 800 mm
	All	$0 < n_{hits} < 20$
Track Selection SSF	All	n_{hits} in tower > 7
	All	n_{hits} in layer < 3
Track Selection BL	All	n_{hits} in tower > 2
	All	n_{hits} in layer < 3

Table 6 – Selection cuts for each electron runs.

Name	**Beam Energy**	**Cut**
Event Quality	All	Cherenkov ON
	All	Energy in the first 3 layers of AHCAL $>$ 10 MIP
Electron Selection	10 GeV	$25 < n_{hits} < 75$
	15 GeV	$30 < n_{hits} < 90$
	20 GeV	$40 < n_{hits} < 100$
	30 GeV	$50 < n_{hits} < 110$
	40 GeV	$60 < n_{hits} < 120$
	50 GeV	$70 < n_{hits} < 140$
	All	$cog_z <$ 250 mm
	All	-90 mm $< cog_{x,y} <$ 90 mm
	All	Energy in last two layers $< 1\%$ E_{sum}

Table 7 – Selection cuts for the pions runs.

Name	**Beam Energy**	**Cut**
Event Quality	All	Cherenkov OFF
Pion Selection	All	$n_{hits} > 20$
	All	n_{hits} in the first 2 AHCAL layers < 5
	All	Energy in last two layers $> 1\%$ E_{sum}
Multi Particle Rejection	All	n_{hits} in time window > 5
	All	$n_{Cluster} > 0$